DEFECTS IN METALS AND SIMULATION OF MECHANICAL PROPERTIES BY MEANS OF NANOINDENTATION

By

ELIAS K. NJEIM

A thesis submitted in partial fulfillment
of the requirements for the degree of

MASTER OF SCIENCE IN MECHANICAL ENGINEERING

WASHINGTON STATE UNIVERSITY
School of Mechanical and Materials Engineering

DECEMBER 2009

To the Faculty of Washington State University:

The members of the Committee appointed to examine the thesis of ELIAS K. NJEIM find it satisfactory and recommend that it be accepted

_____

David Bahr, Ph.D., Chair

_____

Hussein Zbib, Ph.D.

_____

Sinisa Mesarovic, Ph.D.

ACKNOWLEDGMENTS

The time and commitment of my advisor Dr. David Bahr for the duration of my research was greatly appreciated. The author would like to thank Idaho National Labs for the financial support. The author would like to acknowledge Dr. H. Zbib and Prof. I. Mastorakos of Washington State University for useful discussions in support of this study.

DEFECTS IN METALS AND SIMULATION OF MECHANICAL PROPERTIES BY MEANS OF NANOINDENTATION

Abstract

by Elias K. Njeim, M.S.

Washington State University

December 2009

Chair: David F. Bahr

Simulations of radiation damage in metals are of real interest when it comes to specifying the effect of radiation in terms of creation of defects such as vacancies, interstitials and dislocations.

Molecular Dynamics is a helpful tool in modeling the process of radiation damage in metals on the small scale, since in MD we have a time scale comparable to the real time scale of radiation damage in metals. Zirconium is an important metal for nuclear applications such as for cladding fuel elements; it has a low absorption cross section for neutrons. We have modeled radiation damage in Zr using the PKA method or Displacement cascades that lead to the creation of defects which evolve with time and lead to changes in microstructure and macroscopic properties. Dependence on temperature and on the energy of the primary knocked on atom were studied; vacancies are the main defects generated for PKA energies ranging from 0.5 to 2 kev, and after around 5 ps of the excitation of the PKA the number of defects starts to stabilize.

In addition, to characterize the effect of defects on the mechanical properties of metals, we have done molecular dynamics simulations of nanoindentation on Iron with vacancies and dislocations separately inside the metal, the effect of indenter velocity and the numbers of vacancies and

dislocations on yield load were also studied; the main results concerning the effect of vacancies and dislocations is that they both lower the yield load of the material during nanoindentation, and a higher concentration of vacancies will cause a higher deviation from the yield point with no vacancies following a weak power law relationship.

TABLE OF CONTENTS

LIST OF TABLES

Page

LIST OF FIGURES

Page

Chapter 1 *Motivation*

The motivation behind this work is to find the effect of defects on mechanical properties of metals and in this way metals properties will be modeled as a function of defects concentration and type, similar to works done by other researchers [1,2,3]. Defects are usually present in metals in different environments, especially in the nuclear industry the materials that are used are to endure severe conditions due to high temperatures and the radiation environment that surrounds the materials. So knowing the effect of the defects on metals will allow the selection of the right metals for the right application.

In this thesis the focus was on investigating the effect of radiation damage on metals and the change in properties that follow the damage. We have used a computational approach to study this problem by means of Molecular Dynamics using the LAMMPS [4] software available online by Sandia Labs, we have chose molecular dynamics since it is a new way to run simulations to model metals that allows a reliable and physical approach to study mechanical properties of metals, we can describe the technique as a "virtual microscope" with high temporal and spatial resolution. Whereas it is possible to take "still snapshots" of crystal structures and probe features of the motion of molecules through NMR, no experiment allows access to all the time scales of motion with atomic resolution. For instance, using Molecular Dynamics to model nanoindetation we can know by means of visualization when the dislocations will form inside the material cell and relate the onset of plasticity to the nucleation and motion of dislocations whereas in an experiment we cannot have a clear picture of the processes happening below the indenter tip. In addition, when we model radiation damage on the atomistic level we can also track the evolution of defects and their interaction. In experiments, since the time scale is much slower, we

basically can do testing on the material after irradiation without having an insight on the miniscule defects generation and interactions.

Background on Molecular Dynamics

Molecular dynamics has been used extensively in Materials Science in general, and specifically to model the materials in the nano-scale, where other tools like finite element fail to predict the mechanical behavior of materials; for instance Chang et al. [5]studied the motion of edge dislocations inside bcc metals and found that Molecular Dynamics provides a direct and practical means of calculating dynamical properties of dislocations in metals and was able to obtain an array of velocity data for various temperatures and shear stresses. In addition to studying miniscule mechanisms Molecular Dynamics can provide means of studying the mechanical properties of metals; for instance Qizen Li [6] used a different approach that focused on studying the mechanical properties of thin films with dislocation sources using MD .

In another scheme Altshuler et al. [7] studied hydrogen diffusion on BCC metal (110) surfaces using Molecular Dynamics with a focus on temperature and coverage effects and they found a higher diffusion with increasing temperature. In addition Farid F. Abraham [8] studied crack dynamics in brittle fracture using molecular dynamics. Those examples show that Molecular Dynamics has been successfully applied many applications, and therefore is a likely method to investigate the mechanisms which may be of interest in controlling micromechanical behavior of materials.

In Molecular Dynamics, we have a dimensional scale in the order of multiple nanometers and the time scale on the order of picoseconds. While this makes it hard to compare directly to

experiments, the advantage is that we can trace the different stages of short lived processes that happen in a short time and we can visualize how the defects interact and change in this period.

In addition, Molecular Dynamics provides the option to make different types of mechanical tests on metals like Nanoindentation [1,9,10,11] and shear tests [12] and to get results comparable to experiments. In previous works in MD with nanoindentation were focused on the onset of plasticity and on the effect of different types of defects on yielding, in fact in [1] the effect of voids on the yield load during nanoindentation was studied and the position of the void away from the indentation surface was varied, in addition in [10] the critical shear stress for the onset of plasticity in Cu was determined using nanoindetation. In [12] the ideal strength of iron in tension and shear was studied and their results showed compatibility to the results in chapter 2 which examines the load required to initiate plastic deformation in iron as a function of vacancy concentration.

The drawback of Molecular dynamics is that the simulations cannot sample time scales beyond nanoseconds, since the timestep is on the order of picoseconds. Simulations require a high processing power and still the simulations could take a long period of time. The timestep which is the time length between evaluations of the potential, it must be chosen small enough to avoid discretization errors. Typical timesteps for classical MD are in the order of one femtosecond [13].

It is also worth noting that other methods of modeling could have been used, like the finite element method where a constitutive model should be defined for the specific type of material before running the simulation. FEM simulations are mainly focused on the bulk behavior of materials under testing, while our interest was more into mechanisms that were modeled using

atomistic simulations without the pre-definition of a set of equations for a certain constitutive model.

This thesis will explore the interactions of defects in metals with the resulting mechanical properties. In chapter 2 the focus will be on the effect of vacancies on the mechanical properties of BCC Fe having the vacancy concentration and the indenter velocity as variables. In chapter 3 defects generation by irradiation damage using molecular dynamics to model displacement cascades in Zirconium HCP will be the subject matter; with emphasis on defects evolution with time and having the temperature and the primary knock on atom initial energy as variables. In chapter 4 the focus will be on the effect of dislocations on onset of plasticity of BCC Fe.

Chapter 2 *Vacancies effect on metals mechanical properties*

Nanoindentation has become a common experimental technique for assessing the mechanical properties of metals; both the propagation of a well developed plastic zone and the nucleation or activation of dislocations can been probed with this technique. The onset of plasticity during nanoindentation is often associated with dislocation nucleation in a wide range of metallic systems [14,15,16]. Schuh et al. [9] has noted that atomic-scale mechanisms that control incipient plasticity may be related to vacancies and their interaction with defects and shown evidence of this using temperature controlled indentation in platinum. BCC metals, however, have shown less sensitivity to temperature [17]. With observations of the role of dislocation nucleation on the deformation of small structures using electron microscopy [18], there is growing interest in identifying the role dislocation nucleation plays in plasticity in small structures. Complementary molecular dynamics (MD) simulations have been carried out by a number of researchers to assess the mechanism of dislocation nucleation that has been hypothesized in the literature during indentation [19,5]. Studies of defect free tungsten support the nucleation model and have verified that in some cases the loading prior to the yield point is purely elastic [20].

Many simulations of indentation systems, however, have considered only systems which are either structurally or chemically perfect. There are fewer examples of experimental [11,21]and simulation studies of small scale defects using these methods. Shan *et al* [1] conducted molecular dynamics simulations to study the effect of voids on the mechanical properties of single crystal Cu. Chang and Chen [22] have demonstrated that MD is likely a more suitable method to study this level of small scale deformation than molecular statics by simulating a uniaxial tensile test of copper nanowires. Mukherjee *et al* [3] studied the effect of interstitials and vacancies on the indentation-induced plasticity and reasoned that the vacancies annihilate

during nanoindentation using a two dimensional close-packed array of "straws". This current chapter investigates the effect of vacancy concentrations on the load required to cause the onset of plasticity (i.e. dislocation nucleation) during nanoindentation on single crystal Fe using molecular dynamics simulations.

Nanoindentation simulations were performed on a simulation cell of single crystal Fe 150 Å wide by 150 Å long by 100 Å thick, enclosing 199439 atoms using LAMMPS [4]. The crystal was composed of Fe modeled with the FS Embedded Atom Method potential [[23]]. Periodic boundary conditions were used in the x and y directions while the top surface was traction free and the underside was held fixed. The nanoindentation was performed using the NVE ensemble. A rigid spherical indenter was used, with a radius of 40 Å; the indenter exerts a force of magnitude $F(r) = -k(r-R)^2$ on each atom where k is the specified force constant, r is the distance from the atom to the center of the indenter, and R is the radius of the indenter. The force is repulsive and $F(r) = 0$ for $r > R$, k=100 eV/Å^2, to test the stiffness of the indenter other values for the force constant k of 1000, 3000 and 10000 eV/ Å^2 were used and a slight change in the value of the yield load and in the elastic part of the force displacement curve were noticed The motion of the indenter was prescribed in the z direction with a constant velocity; simulations using 100 m/s and 20m/s velocities were studied. The arrangement of the orientations of the single crystal is x [100] y [010] and z [001]; nanoindentation was performed on the Fe (100) surface. The temperature was initially set to 0 K and changes in temperature during nanoindentation were recorded, the temperature fluctuating between 0 and 5 K for the elastic portion of the indentation and increased to approximately 13 K after reaching the yield load. Fig. 2-1 shows the atoms below the indenter at an indentation depth of 7 Angstroms,

showing no dislocation nucleation below the indenter tip which proves that the deformation was elastic until they yield load was reached at a depth of 13 Angstroms.

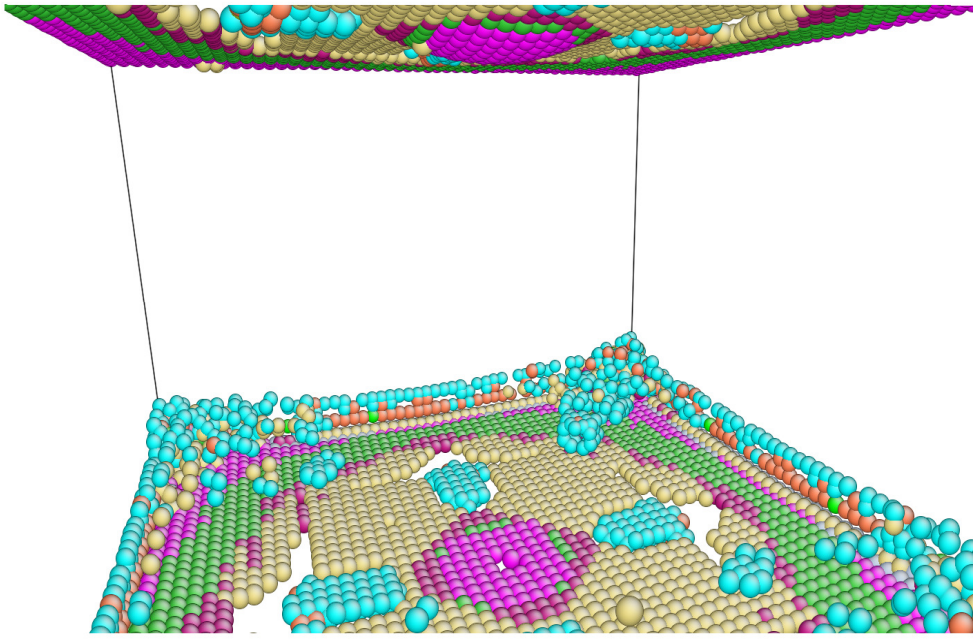

Fig. 2-1: Penetration of indeter at a depth of 0.7 nm. The figure shows only atomic positions that do not meet the coordination number of 8: the indenter is applied to the top of the cell in this figure

The temperature increase is most likely due to phonon generation from the motion of dislocations. Different concentrations of vacancies inside the simulation box were created by specifying a fraction of atoms to be deleted within the simulation box and the atoms deleted were chosen randomly, all vacancy fractions noted in this paper are in atomic percentage, in fact J.H. Schneibel [24] explained that a vacancy concentration of 0.2 % is a relatively high concentration of vacancies when investigating the effect of Nickel alloying on iron aluminides, which proves that our concentrations range was in context with other experimental approaches. The initial contact position of the indenter probe always remained at the center of the simulation cell. Fig. 2-2 shows one of the random vacancies distribution inside the simulation box.

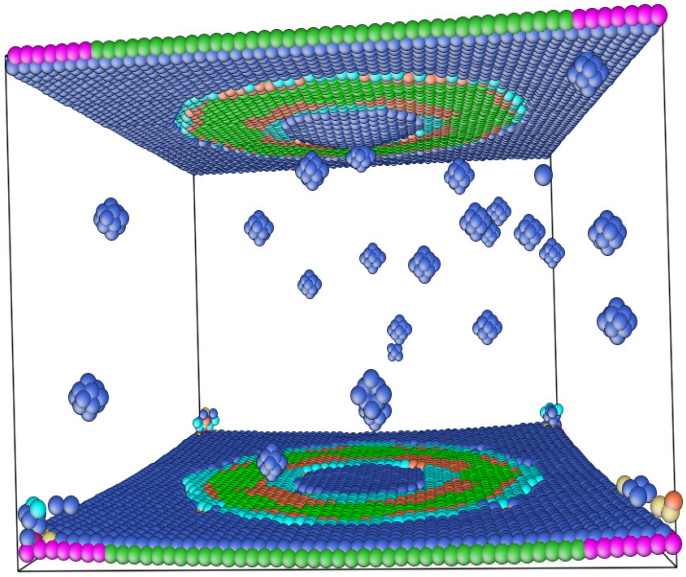

Fig.2-2: Position of randomly created vacancies inside simulation box at a penetration depth prior to plasticity; indenter force is applied on the top of the simulation cell (atoms with a coordination number less than 8 are shown in colors, all other atoms are removed)

Taking into consideration the effect of indenter velocity on the yield load of the force-displacement curve; force displacement curves for 20m/s and 100m/s are plotted on the same graph in Fig. 2-3.

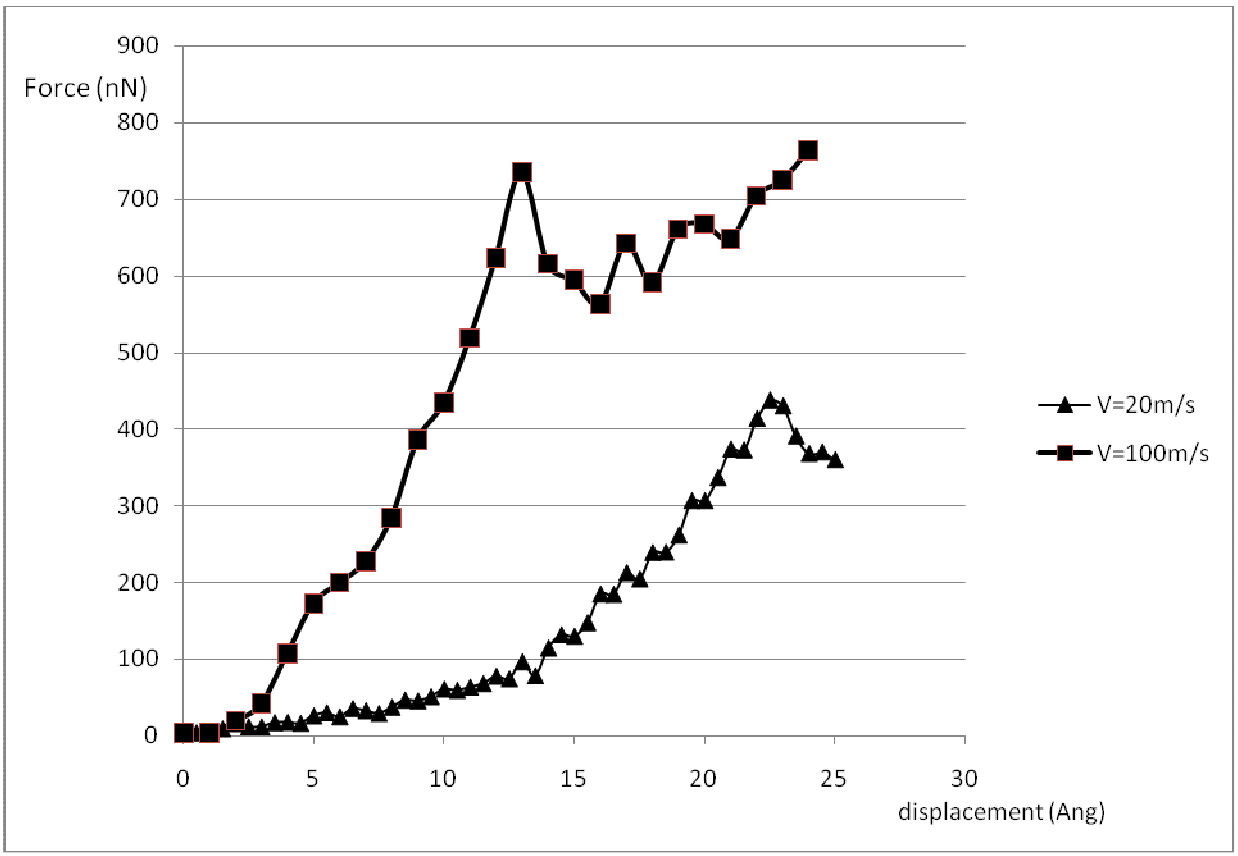

Fig. 2-3: Force displacement curves for indenter velocities of 20 and 100m/s with no vacancies.

As expected Fig. 2-3 shows that the yield load decreases as the velocity of the indenter decrease, comparable to what was observed by other investigators [25] where the yield stress decreased with a lower strain rate. In addition Te-hua Fang et al. [26] investigated the atomistic mechanism of nanoindentation process under various indentation loads and velocities using a diamond tip penetrating a copper thin film, they found that at higher indentation velocities the Young's modulus and hardness increase, which explains the difference in the elastic part shown in Fig. 2-3 for different indentation velocities in iron.

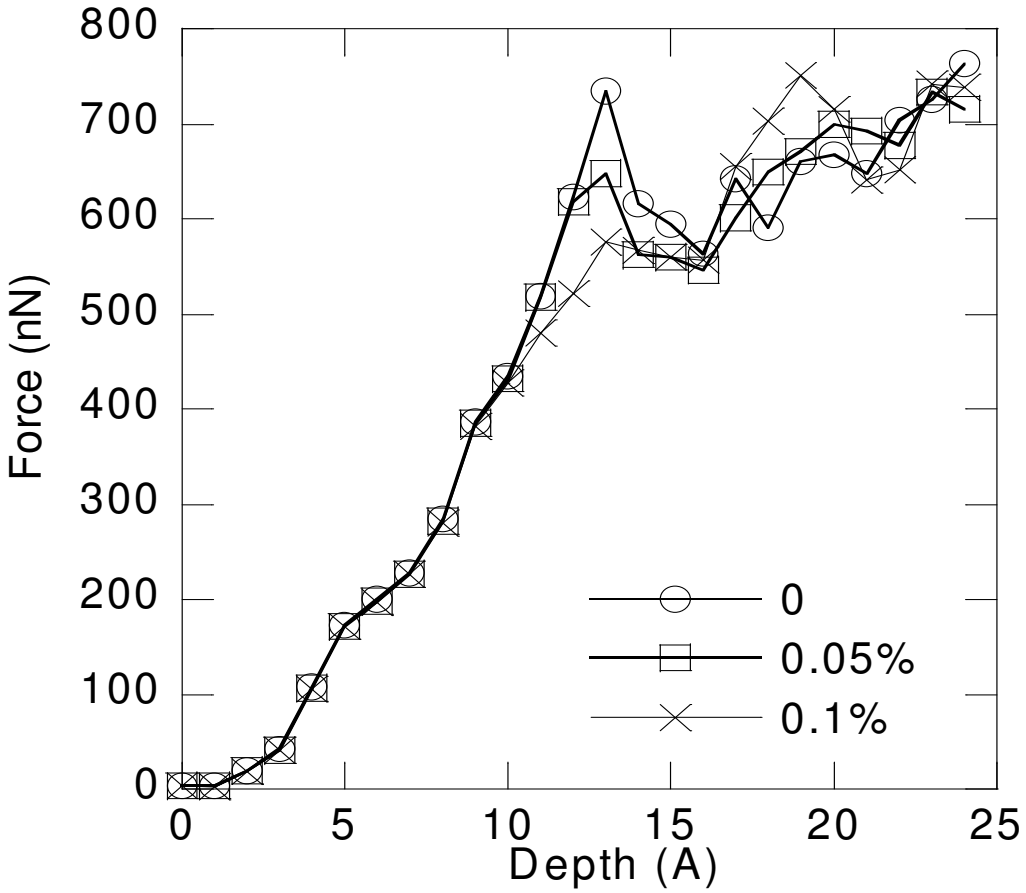

Fig.2-4: Load-depth curves for three vacancies fractions showing decreased yield load with increasing vacancy concentration.

Load – displacement relationships for indentations at 100 m/s for the perfect Fe crystal and with vacancy concentrations of 0.05 and 0.1 % are shown in Fig.2-4. In general, the elastic loading is relatively independent of vacancy concentration at these concentrations, as it is expected that vacancies would have no significant effect on the elastic deformation. At a depth of 13 Å the material starts to yield for the three curves; the load drops with increasing penetration depth. This indicates the start of the plastic regime where dislocations are created and start to move. Additionally, at this point the sample exhibits a rise in the temperature from 5 to 13 K, which is physically explained as the result of the motion of dislocations that causes friction and subsequently a rise in the temperature.

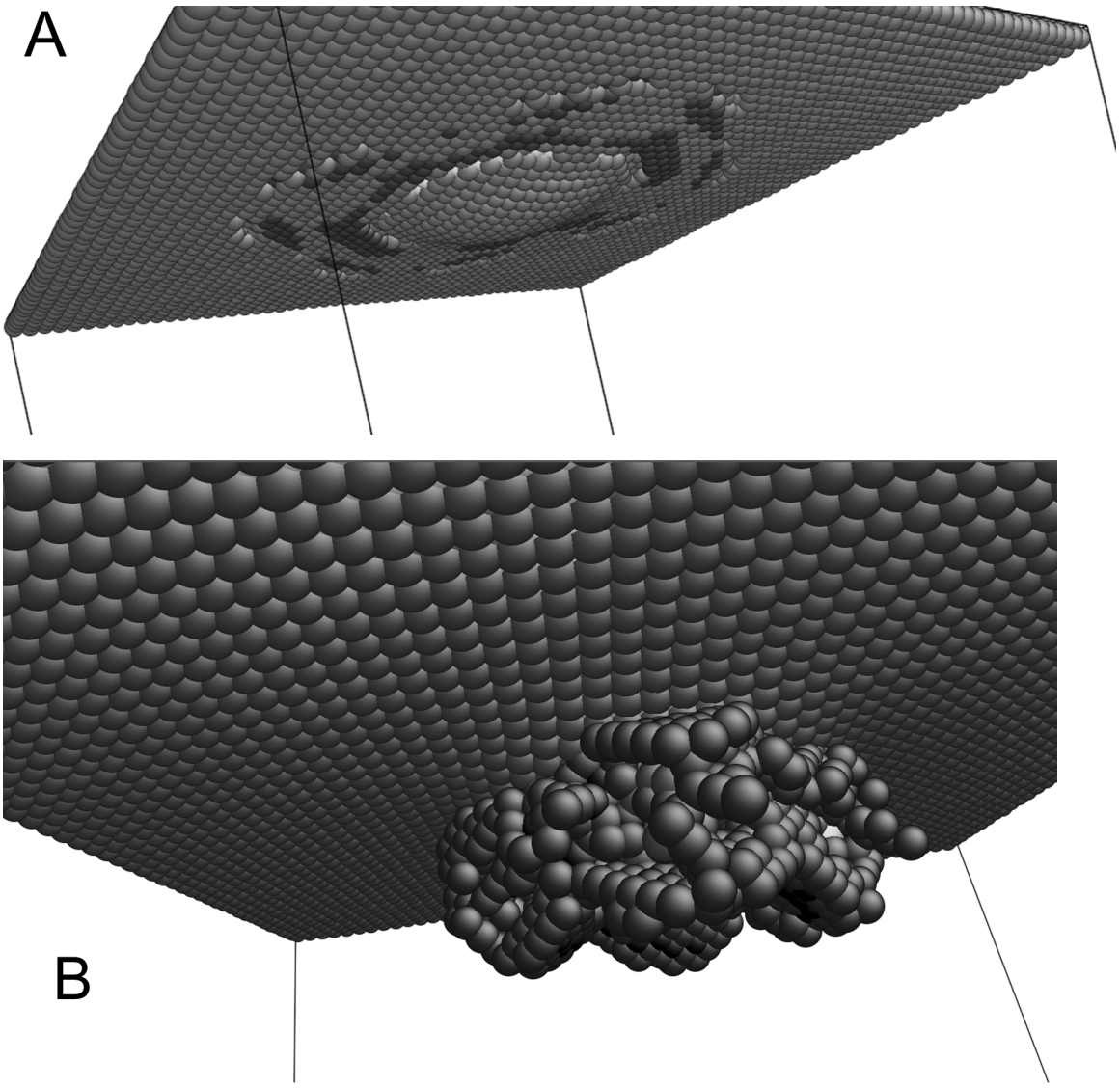

Fig.2-5: Indentation with 0% Vacancies at a) a depth of 9Å showing atoms with decreased number of nearest neighbors b) View at the yield load with depth13 Å. The large cluster of atoms with co-ordintation numbers less than 8 is representative of dislocation formation.

Fig.2-5 shows two snapshots of the atoms at two different depths of the indenter for 0.0% vacancies. To visualize the deformation, Fig. 2-5 only notes atom positions which do not have a coordination number of 8, the typical value for BCC materials. Fig. 2-5(a) shows the surface deflection as a result of the force exerted by the indenter showing no plastic deformation and no

dislocations at a penetration depth of 9 Å, while Fig. 2-5 (b) shows the atomic arrangement at a depth just after 13 Å, where dislocations have clearly formed.

Snapshots at two different depths of the indenter for 0.05% vacancy concentration are shown in Fig. 2-6

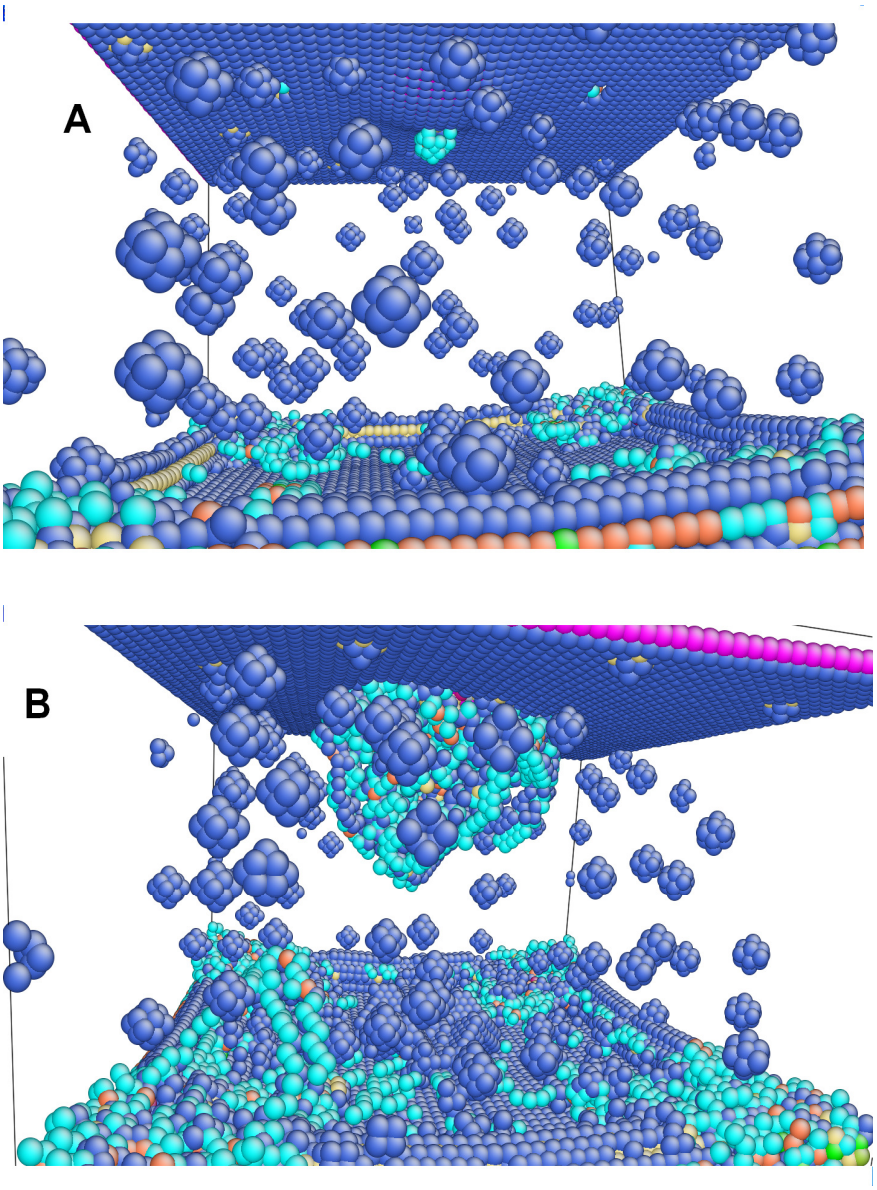

Fig.2-6: Indentation into solid with 0.05% Vacancies a) View at a depth of 9Å showing atoms with decreased number of nearest neighbors b) View at the yield load with depth13 Å.

In Fig. 2-6 a) and b) we can see that the vacancies are moving toward the indentation surface and at the yield load vacancies combine with nucleating dislocations which explains the decrease in the yield load when having dislocations inside the simulation cell.

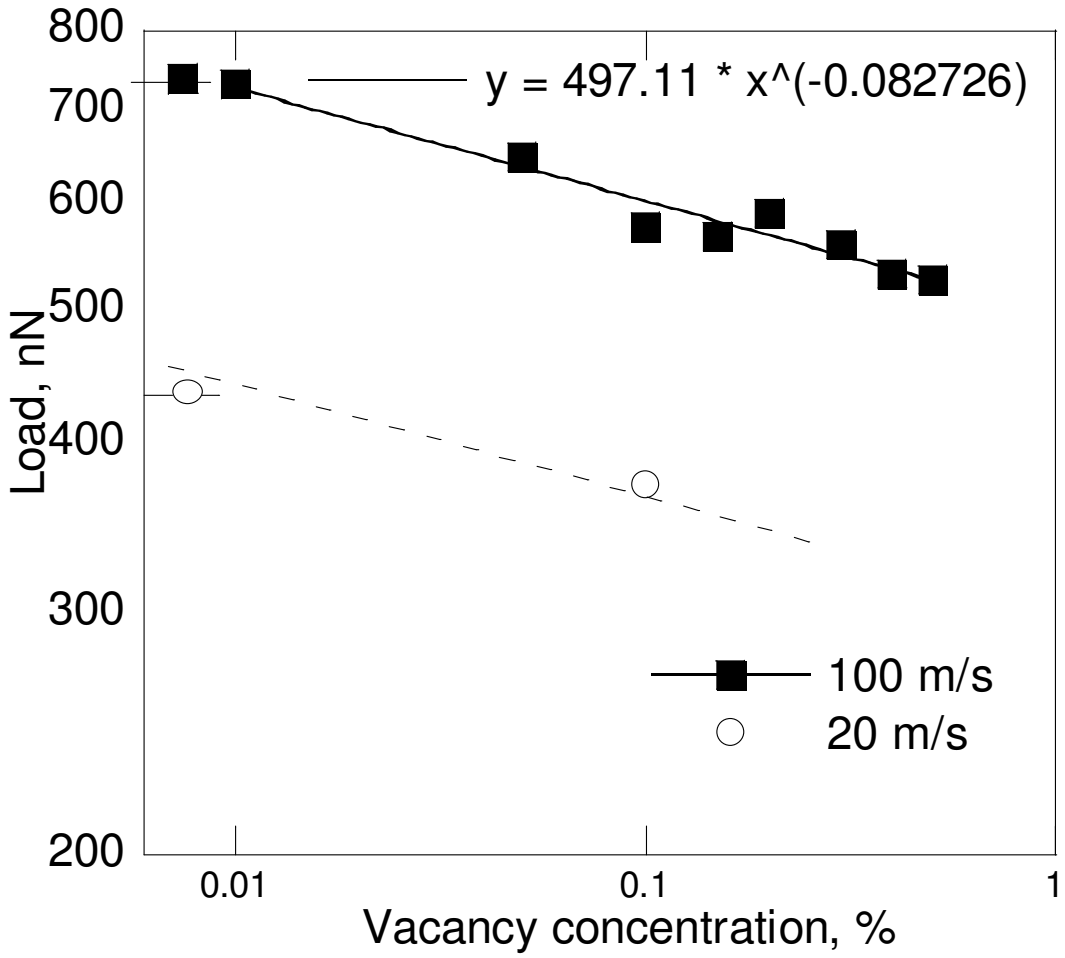

Fig.2-7: Yield loads for different vacancies concentrations and for two different indentation velocities 100m/s and 20m/s

The results of MD simulations run at various vacancy concentrations and penetration rates, and tracking the load at which the first evidence of plastic deformation occurs are shown in Fig. 2-7. In general, the load at yielding decreases with increasing vacancy concentration at concentrations above 0.01%. The relation between the yield load versus the vacancy

concentration follows a power law of the order of ~ -0.1. Multiple simulations at a given concentration vary by less than 5%.

To give an insight about the effect of having a random distribution of vacancies on the yield load we show in Fig. 2-8 multiple runs for same vacancies concentration but for different random distributions of vacancies; the effect of the random distribution are minimal and the maximum difference in yield load is around 5%.

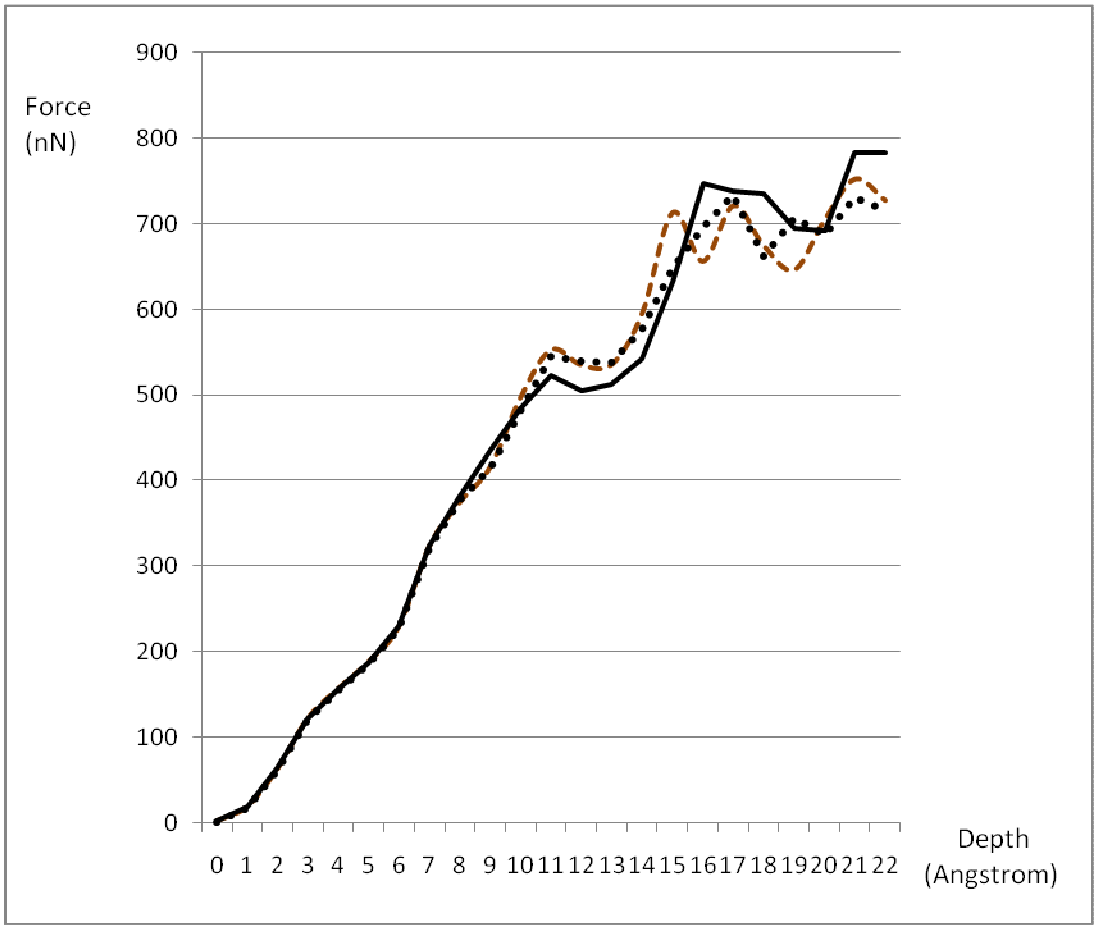

Fig. 2-8: Load displacement curves from multiple runs for the same vacancy concentration of 0.1% with different vacancies distributions, showing variability from random positioning of the defects.

Vacancy concentrations were varied from 0% to 0.5% and nanoindentation was performed on the simulation cell, Table 2-1 shows the force displacement data for those different concentrations for a temperature of 0 k and an indenter velocity of 100m/s.

Vacancy concentration%	0%	0.01%	0.05%	0.1%	0.15%	0.2%	0.5%
Displacement (Angstrom)	Force (eV/A^2)	Force (eV/A^2)	Force (eV/A^2)	Force (eV/A^2)	Force (eV/A^2)	Force (eV/A^2)	Force (eV/A^2)
0	2.1951891	2.1357553	2.005451	1.8380473	1.7963498	1.7745307	1.339037
1	2.1481157	2.0675319	1.9533068	1.8290674	1.7521334	1.6676935	0.987603
2	12.162527	11.987372	11.863465	11.641537	11.440648	11.250866	9.485117
3	26.188338	26.112995	25.895246	25.592269	25.404432	25.26448	24.07578
4	66.775687	66.68276	66.465239	65.861366	65.555284	65.416923	63.79127
5	107.93385	107.78065	107.231	106.88405	106.62029	106.13945	104.9818
6	124.67531	124.19945	123.67099	123.00299	122.70466	122.61465	119.8241
7	142.02304	142.02863	141.48296	141.05381	140.37941	139.80396	136.0409
8	177.77146	177.2304	176.40524	174.90058	174.49612	173.74854	168.4024

9	240.95953	240.82245	240.25372	238.17445	238.30416	237.83061	229.0971
10	271.01541	270.87214	269.69406	266.66397	265.84161	266.61996	251.6861
11	323.80929	324.41358	323.20738	299.62626	299.20775	304.29487	269.620
12	389.05075	389.6044	385.76087	325.07024	322.75769	321.9736	312.705
13	458.92977	456.68196	404.2042	359.27666	354.13484	367.54345	329.010
14	384.4952	362.79402	350.82621	353.97988	328.31781	323.01091	323.01
15	371.0621	350.95839	349.71724	349.80942	356.11727	357.63725	314.544
16	351.79885	355.09824	341.16642	347.11954	381.10334	356.06919	374.631
17	401.09102	372.79327	375.23951	408.88373	428.60234	422.73653	407.937
18	369.07065	403.30067	405.41195	438.46963	434.08928	429.30625	462.25
19	412.58207	414.08835	418.72384	468.34814	448.8335	447.86746	461.770
20	416.5906	413.26433	436.29501	446.25063	474.10852	438.8806	452.713
21	404.66194	398.01901	432.46904	400.04653	403.47455	367.36748	420.924
22	439.68343	391.83363	423.15253	406.48696	420.11292	426.5998	425.85
23	452.80136	414.08943	458.06022	462.67755	426.56529	417.45909	464.213
24	476.81	404.68585	446.70852	461.11334	434.64622	435.26709	444.086

Table.2-1: Force Displacement Data for simulations with different vacancy concentrations.

The load at yielding is also sensitive to indentation velocities, with 20 m/s yielding at loads substantially lower than at 100 m/s for the same vacancy concentrations. This is similar to the work of Schiotz [27] who studied the plastic deformation of nanocrystalline copper, in which reductions in the strain rate by a factor of 10 caused a15 % reduction of flow stress. If the same mechanism of yielding is present at the strain rates where experimental tests are performed, it will be expected to exhibit a similar mild decrease in yield point phenomena with vacancy concentration.

While the simple Hertzian approximation for spherical indentation is not strictly valid at depths that are significant fractions of the contact probe radius [28,29], for simple comparisons to other published results a first order approximation of the maximum shear stress, τ_{max} under the indenter tip can be made using

$$\tau_{max} = 0.31\left(\frac{6(E^*)^2}{\pi^3 R^2}\right)^{\frac{1}{3}} P^{1/3} \qquad \textbf{(1).}$$

From the data presented in Fig. 2-7, the typical; shear stress from (1) is on the order of 7 GPA for defect free crystals; similar to that proposed by other investigators [12].

It s important to show a Hertzian fit along with our simulations with different indentation different values of indenter stiffness K, in Fig. 2-9 we show a Hertzian fit for the force displacement curve along with previous curves that were obtained.

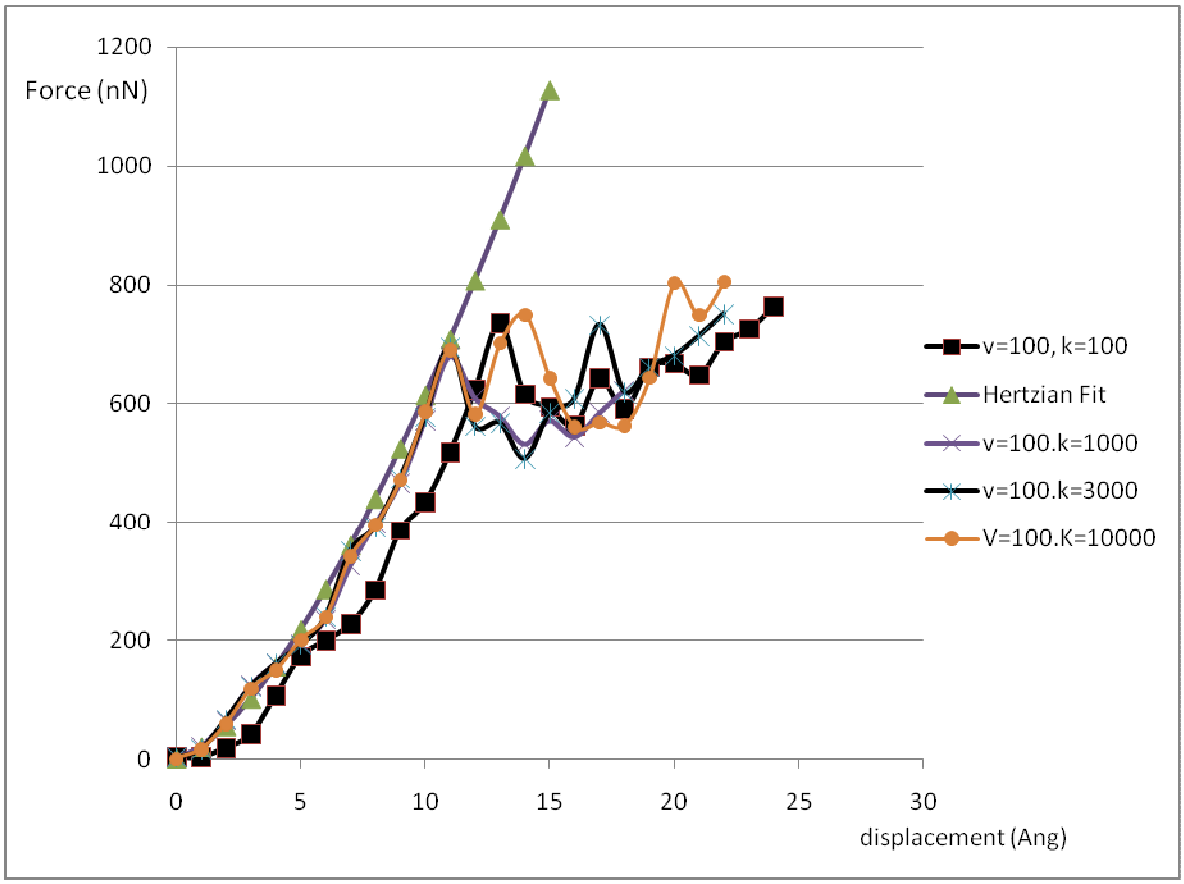

Fig. 2-9: Hertzain Fit and load displacement curves from simulations for different values of the force constant K (indenter stiffness)

The equation used for the Hertzian force displacement fit is:

$$F = \frac{4}{3} E^* R^{1/2} d^{3/2}$$

$$\frac{1}{E^*} = \frac{1-\nu_1^2}{E_1} + \frac{1-\nu_2^2}{E_2} \quad [30]$$

F is the load, d is the depth inside the sample

R is the spherical indenter radius

E1, v1 are respectively the elastic modulus and poison's ratio of the sample

E2 and v2 are the elastic modulus and the poison's ration of the indenter (with k>1000 the indenter is perfectly rigid)

Fig. 2-9 shows that with a higher stiffness (k=1000 eV/ $Å^2$ and above) of the indenter is very close to the Hertzian fit in terms of force and displacement values, which is a proof that the system during nanoindentation behaves as it s supposed to behave during experimental nanoindentation.

In summary, the effect of vacancies on the yield load in nanoindentation was studied by molecular dynamics simulations. The results indicate that the presence of vacancies lowers the yield load, and a higher concentration will cause a higher deviation from the yield point with no vacancies following a weak power law relationship. During nanoindentation we can observe that the number of vacancies is going down as the indenter depth is higher.

Dislocations begin to form at the yield load and after this point the model behaves plastically. The vacancies are not required to be present at the regions of highest imposed shear stresses to impact the nucleation stress, and as such may be influencing the stress field in the solid as well as participating directly in mechanisms that require additional time or temperature to activate a source.

Chapter 3 *Radiation damage in metals*

In the previous chapter vacancies were introduced artificially into the lattice. However, in actual service a very likely mode of vacancy introduction is the interaction with solids and radiation, and so in this chapter the interaction of a metal with a radiation environment will be examined.

A collision cascade is a set of nearby adjacent energetic collisions of atoms induced by an energetic particle in a solid or liquid [31,32], when an energetic particle penetrates a solid, it loses its energy by a series of elastic nuclear collisions and through excitations of the electronic system. Below 10 Kev elastic collisions are most important, elastic collisions set into motion target particles, which can in turn displace neighboring atoms which creates a displacement cascade [33]

If the maximum atom or ion energies in a collision cascade are higher than the threshold displacement energy of the material, the collisions can permanently move atoms from their lattice sites and produce defects. The initial energetic atom can be e.g. an ion from a particle accelerator, atomic recoil produced by a passing high-energy neutron, electron or photon, or can be produced when a radioactive nucleus decays and gives the atom a recoil energy. The nature of collision cascades can vary strongly depending on the energy and mass of the recoil/incoming ion and density of the material.

Cascade modeling deals with the effect of a high velocity particle impact on a solid. These simulations are of major interest in the nuclear engineering domain as they are major tools to analyze the behavior of materials subjected to irradiation [33].

Atomistic computer simulation techniques have become powerful enough that many phenomena connected to radiation damage effects in metals can be modeled with a high level of practicality. This thesis will present a study of this phenomenon using the Primary knock- atoms that recoil under impact from energetic atomic particles such as neutrons or ions are the principal source of damage. At high enough recoil energy, they create cascades of atomic displacements that result in self-interstitial and vacancy defects. The time and length scales of the cascade process are ideally well-matched to atomic-scale computer simulation by molecular dynamics. MD is also being used to reveal the nature of the motion and interaction of defects. The effect of the Energy of the PKA and the effect of the simulation temperature on the number of defects are studied.

In this chapter, radiation damage in Zirconium is studied since it is an important metal for nuclear applications such as for cladding fuel elements; it has a low absorption cross section for neutrons. In addition Zirconium is exceptionally resistant to corrosion. Other studies have been carried out in more common engineering alloys [34,35], and so the use of Zr has been chosen to explore a new system while developing the tools needed for further studies between vacancies and mechanical stresses.

The cascade damage caused by radiation on single crystal Zirconium HCP, displacement cascades, which are the primary result of radiation on a metal, were modeled using molecular dynamics.We have used the software by Sandia Labs "LAMMPS" [4], where we provide the input script to the gauss server available at WSU and LAMMPS runs our commands in a parallel computation manner on different computer processors. Displacement cascades lead to the creation of defects which evolve with time and lead to changes in the microstructure. Dependence on temperature and on the energy of the primary knocked on atom were studied and discussed.

The simulation box has a rectangular shape with dimension of [96.6 96.6 161] Angstroms. Periodic boundary conditions at constant volume were applied along all three principal axes. The simulations were carried at two different temperatures, 300K and 400K, and the number of atoms in the simulation box was selected in accordance with the primary knock-on atom energy, temperatures during the hit were almost stable with no major fluctuations. Our systems are set to satisfy the statistics of the microcanonical ensemble NVE, in the NVE ensemble the system is isolated from changes in moles (N), volume (V) and energy (E), the NVE ensemble was recommended for Cascade Modeling by J. P. Crocombette [33].

The Primary Knocked on atom energy was varied between 1 Kev to 3 Kev for both temperatures, other investigators used a range of PKA energies that varied from 0.5 Kev to 100 Kev and sometimes more, for instance G. R. Odette et al.[36] showed the average number surviving defects as a function of PKA energy, their numbers make a correlation with the numbers found for cascade modeling found for Zirconium.

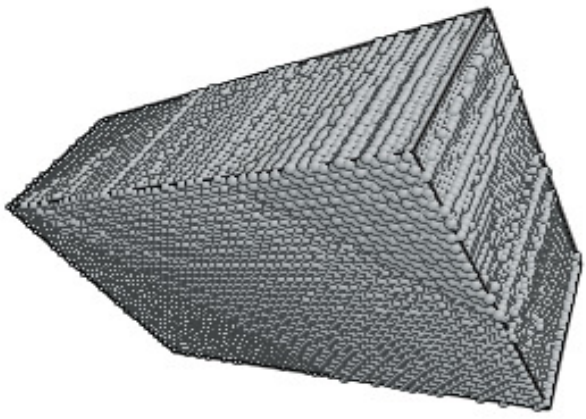

Fig.3-1: Simulation Box for Zirconium HCP

Figure 3-1 shows the simulation box created using the HCP structure for Zirconium, potentials for Zirconium [37] from the LAMMPS library of potentials were used.

Lattice parameter (A)	**Simulation box dimensions (A)**	**Timestep (picoseconds)**
3.22	**[x=96.6 y=96.6 z=161]**	**0.001**

Table.3-2: Simulation of radiation damage in Zirconium constants.

Results and Discussion

At the start of the simulation a file is set to assemble the output of the simulation. This allows the number of vacancies to be measured as a function of time, and have snapshots of the simulation box. This means the formation and annealing of defects can be measured.

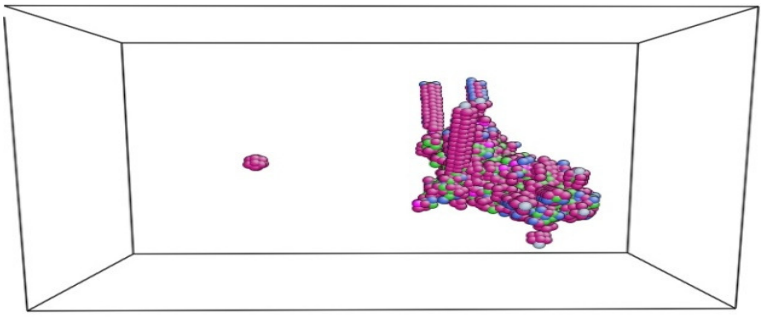

Fig. 3-2: Defects formation at the beginning of the simulation. Atoms with a non-perfect co-ordination number are shown as colored atoms, all other atoms removed.

Fig. 3-2 shows the start of the radiation damage process where defects start to form in a relatively large amount, the first defect on the left of the figure is where the PKA started and the large number of defects created are on the right side

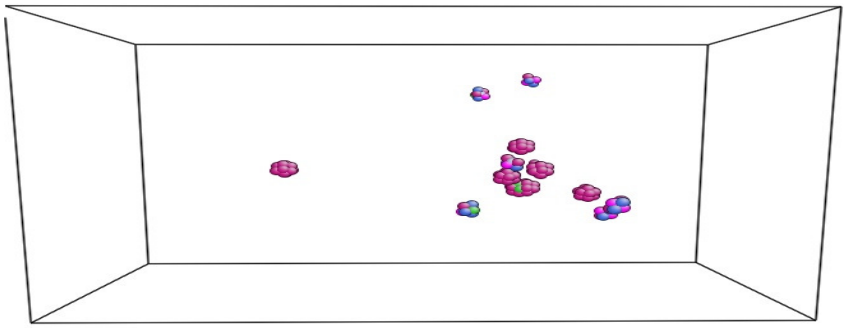

Fig.3-3: Vacancies and interstitials after annealing (~5ps). Atoms with a non-perfect co-ordination number are shown as colored atoms, all other atoms removed.

In Fig. 3-3 we can see the defects that survived after a time of 5 picoseconds, which means that those defects will stay in the material while the other defects that we saw in fig. 3-2 have annihilated, those defects that we see are mainly Vacancies and Interstitials.

The evolution of defects with time in between the first picoseconds and 5 picoseconds is shown in a series of snapshots taken in between the two times in Fig. 3-4:

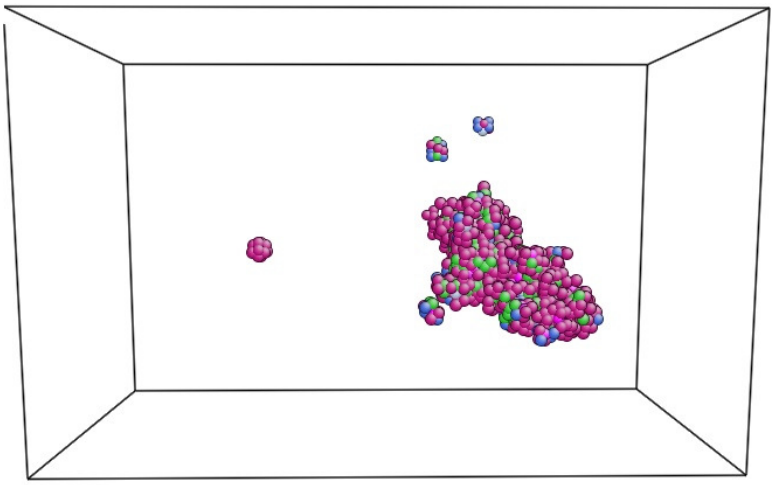

Fig. 3-4a: Defects after the initiation of the PKA (ta<5ps), only atoms with a non-perfect co-ordination number are shown.

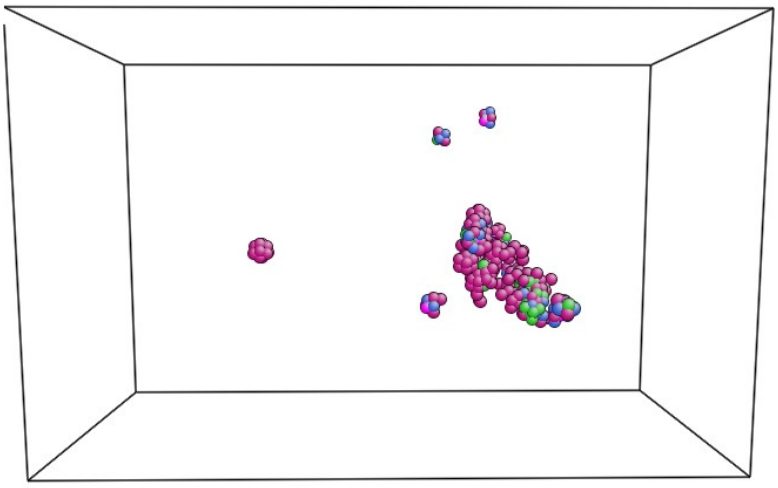

Fig. 3-4b: Showing defects after fig. a showing how the defects evolve (tb<5ps)

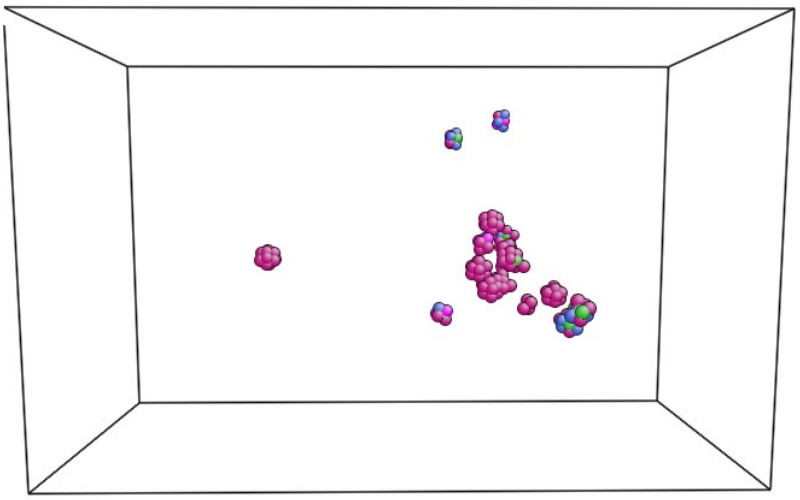

Fig. 3-4c: Showing the defects after fig. b showing how defects evolve (ta<tb<tc) (tc<5 ps)

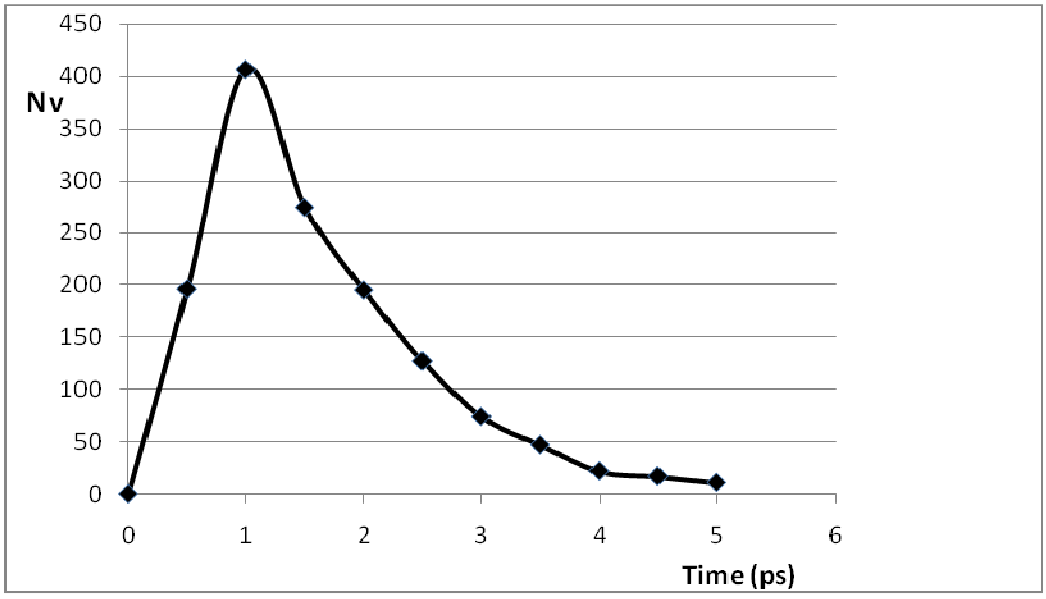

Fig.3-5: The evolution of the number of vacancies inside the simulation box as a function of time

In Fig. 3-5 we can see the evolution of the number of vacancies after the initiation of the PKA as a function of time, the first thing to note is that the number of vacancies decreases exponentially and stabilizes to a fixed number in a period of around 5 picoseconds as has been shown in studies conducted on metals undergoing radiation damage [38,39,40], for instance Carlos Campañá et al. [38] studied radiation damage in Fe bcc and showed that the defects stabilize and reach a stable configuration in around 5 picoseconds, the majority of vacancies were singular with a small proportion of divacancies.

Relating Fig. 3-4a, 3-4b and 3-4c to the graph in Fig. 3-5 that shows a remarkable decrease in the number of defects after passing the 1 picosecond period, makes a good correlation in terms of numbers of vacancies decreasing as simulation time increases.

The local distortions and electronic changes associated with the formation of vacancies alter the internal energy of the crystal. This increase in energy is balanced with the decrease in energy due to the increase in entropy when vacancies are formed. The total internal energy change associated with n_v vacancies is: $\Delta E = \Delta E_v . n_v$

where ΔE_v is the formation energy of vacancies. At equilibrium the number of vacancies in a system containing N atoms is:

$nv = N \exp(-\Delta E_v / KT)$ [41]

For Zirconium the vacancy formation energy is 1.35 eV and at a temperature of 300 K and total number of atoms in the simulation box N=200000, calculating nv at T=300K $n_v = 4.188.10^{(-18)}$ ~0 vacancies at equilibrium and for T=400K; $n_v = 1.95.10^{(-12)}$ ~0 vacancies at equilibrium. Therefore, for this simulation there would be no expected vacancies at equilibrium within the simulation cell.

The temperature effect on the cascade simulation of radiation damage is of real interest to us since temperature plays an important role when it comes to industrial applications, in the simulation runs that we performed the Temperature (300 K and 400 K) was fixed by rescaling the temperature every 40 steps, and the PKA energy was considered by assigning a velocity to an atom inside the simulation box, the velocity of the PKA can be calculated from the Kinetic energy (KE) of the PKA. The KE of the PKA is related to the Energy (also KE) of the radiation. One way to approximate this relation is by assuming perfect elastic collision between the incoming particle like neutrons and the PKA atom[[42]].

The collision process takes place by the initial particle displacing a Zirconium atom and creating a primary knock-on atom PKA, the recoil energy given to the PKA depends on the particle type and energy. For protons and neutrons the maximum energy Tmax that can be transferred to the PKA is given by [[43]]

$T_{max} = [(4*M*m)/(m+M)^2]*E$

Where E is the energy of the incident proton (or neutron), m is the proton mass and M is the atomic mass of the studied metal, in our case M is the atomic mass of Zirconium.

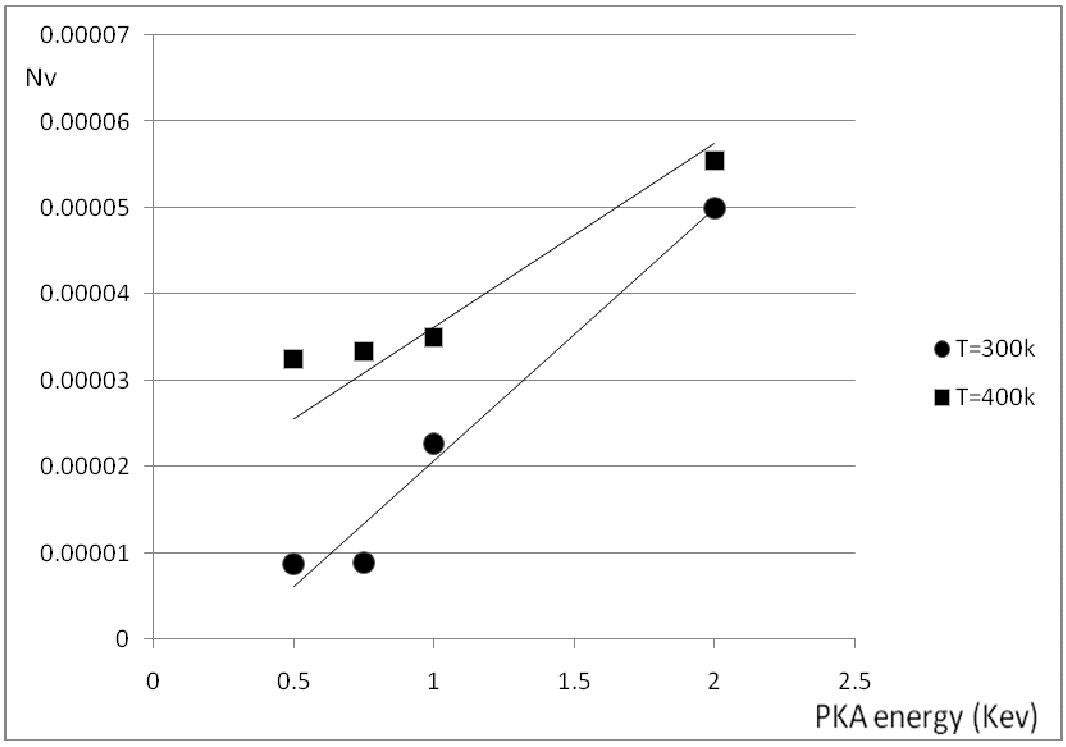

Fig. 3-6: Fraction Nv/n of surviving vacancies as a function of PKA energy (KEV) and of Temperature (K) at 15 picoseconds

Fig. 3-6 shows the fraction of vacancies created out of the total number of atoms as a function of temperature and PKA initial energy. The percentage of vacancies created at the end of the simulation is increasing with the energy of the Primary knock-on Atom for both temperatures of 300 and 400 K, taking into consideration the effect of the temperature on the number of vacancies created, we can see that the percentage of vacancies created is also an increasing function of the temperature since for the same PKA energy but at a higher temperature of 400 K a higher fraction of vacancies is created at the end of the cascade process. The effect of temperature and PKA energy on the percentage of vacancies was also studied in other works by K. Nordlund [34] and A. M. Rutherford and D M Duffy [39], Nordlund studied the relation between the PKA energy and the number of defects on GaN and he showed that the number of

defects is an increasing linear function of PKA energy, slopes of number of defects versus PKA energy were shown and the number of defects for specific energies was in the ranges that we found, not to consider the differences in material properties.

Other investigators used different methods to model radiation damage, for instance L. Yang et al. [44] worked on simulations of displacement cascades using MD in Fe containing different concentrations of substitutional He atoms and studied the effect of He impurities on mechanical properties. For instance they have studied displacement cascades in Fe with different concentrations of He, and they found that the number of point defects increases with both increasing PKA energy and increasing He concentration which does comply with our results for the PKA part.

Chapter 4 *Dislocations effect on Mechanical Properties during nanoindentation*

As in chapter two we studied the effect of vacancies on the mechanical properties of Fe, in this chapter a study on the effect of dislocations on mechanical properties of Fe is presented.

Simulations of nanoindentation were performed on single crystal Fe with similar conditions used in chapter one for vacancies except that the defects introduced in the simulation cell were dislocations.

The concept of a dislocation was first introduced by Orowan [45] and Taylor [46] to explain the discrepancy between the observed and theoretical shear strength of metals, they showed that the motion of dislocations through a crystal lattice requires less stress than the theoretical stress.

Two basic types of dislocations are edge dislocations and screw dislocations, the shear displacements associated with plastic deformation occurs primarily by the movement of dislocations. The slip planes and direction are those of highest atomic density.

It is worth to note previous works that involved nanoindentation and dislocations, in fact H.G.M. kreuzer et al. [47] simulated nanoindentation in discrete dislocation (DD) by the motion of statically distributed discrete dislocations and found that the pre-existing dislocations caused a decrease in the hardness with increasing indentation depth. Other scholars have investigated the effect of dislocation on yielding, in fact Qizhen Li [6] studied the effect of dislocation source length on yield strength of nanostructured metallic multilayer thin films and the general conclusion was that dislocations do lower the yield strength with a focus on the length of the dislocation as a variable.

In this chapter we investigate the effect of a dislocation on the yield load of Iron (Fe) Bcc during nanoindentation. the simulation cell consisted of single crystal Fe 150 Å wide by 150 Å long by 100 Å thick, the orientation of our cell was x [-1 1 0] y [1 1 1] z [1 1 -2], the dislocation was an edge dislocation and was created in the [111] (121) slip system, indentation was performed in the Z direction [1 1 -2] in order to study the effect of the dislocation on the yield load. Periodic boundary conditions were used in the x and y directions while the top surface (Z direction) was traction free and the underside was held fixed. The nanoindentation was performed using the NVE ensemble; indenter velocity was fixed to 1 A/ps (100 m/s) similar to the velocity used previously in chapter 2, the interatomic potential for bcc Fe developed by M.I. Mendelev et al.[48] was used.

In Fig. 4-1 we show the edge dislocation after the relaxation of the simulation box, the dislocation can move in the <111> direction in the (1 1 -2) plane.

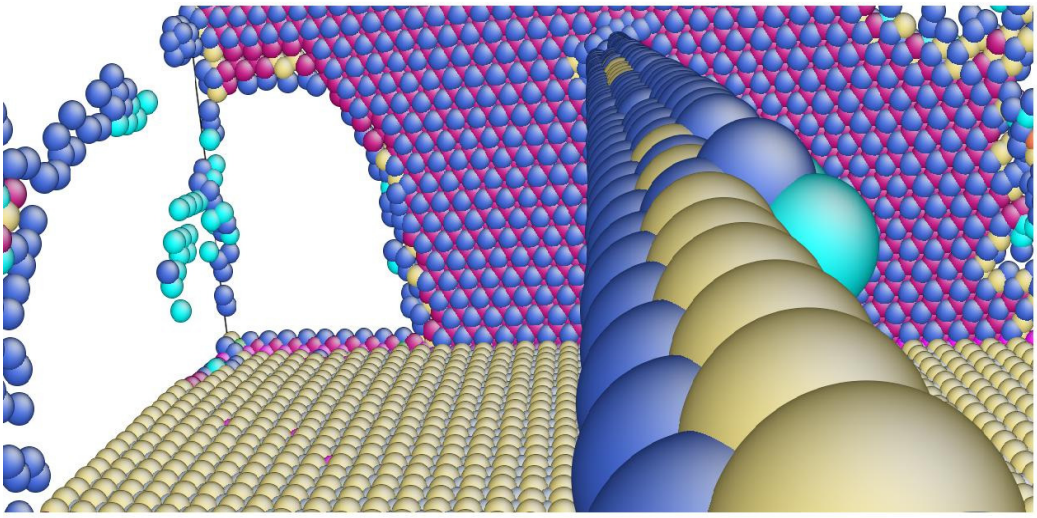

Fig. 4-1: Snapshot of atoms with a co-ordination number less than 8 showing an edge dislocation in the (1 1 -2) plane after relaxing the simulation cell.

The dislocation was created by removing half plane of atoms in the Z direction [1 1 -2], and the simulation cell was relaxed for a certain time until the two planes surrounding the plane that was removed join together, then nanoindentation was performed, the relaxation of the structure was achieved using the conjugate algorithm[49]. In addition, nanoindentation was performed on the same cell without a dislocation to compare the two yield loads with and without the dislocation.

Fig. 4-2 shows the force versus displacement when indenting in the Z direction <1 1 -2> for the two cases, with and without dislocation; there's a decrease in the yield strength when the dislocation is introduced.

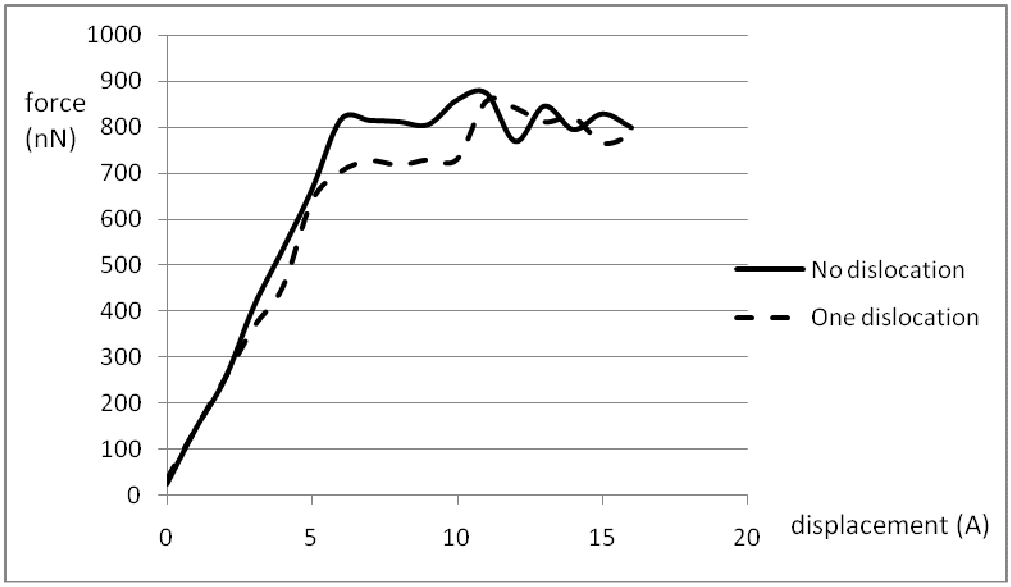

Fig. 4-2: Force displacement for simulation cell with and without a dislocation when indenting the (1 1 -2) plane (Z direction)

In fact the curves in Fig. 4-2 show that for both cases the elastic parts of the two curves are almost the same, but the yield load for the simulation that had a dislocation inside the cell is lower than the other case, what is also worth mentioning is that after yielding; in the plastic part of deformation, the two curves follow the same path. The load displacement curve for the

existing dislocation deviates from the other curve at a load of around 300 nN which is suggested by Johnson [30,50] who suggested that when the stress field around a contact load generated by the application of a load-controlled testing system encounters an existing dislocation; there could be a gradual yielding in which the curve gradually deviates from the elastic loading curve and exhibits increasing amounts of plasticity, this description fits the result shown in Fig. 4-2.

Considering the case when nanoindentation is performed in the <1 1 -2> direction (Z direction) as shown in Fig. 4-3; the important aspect is that the dislocation didn't move in the its slip plane since the load is applied in a direction <1 1 -2> that the dislocation does move on, so the dislocation stayed fixed in its initial position, but still Fig. 4-2 shows that even if the dislocation is not moving during elastic deformation its effect on yielding is important, which brings the idea of the effect of the stress field around the dislocation that has its effect on the nucleation of new dislocations under the indenter tip and subsequently on the onset of plasticity or the yield load.

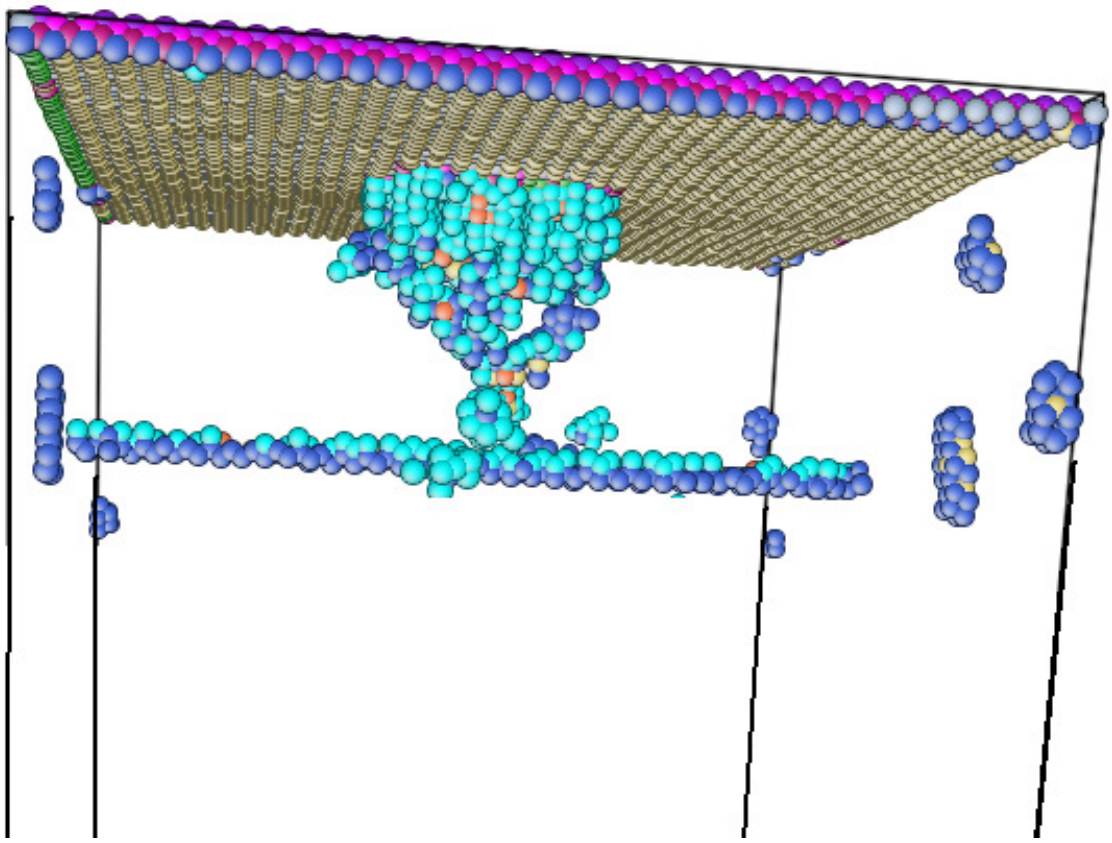

Fig. 4-3: Edge dislocation in the (1 1 -2) plane while indenting in the Z <1 1 -2> direction, yielding at a depth of 7 A. Atoms with a co-ordination number less than 8 are shown. All other atoms are removed.

Fig. 4-4 shows the same scenario as Fig. 4-3 but at a higher depth; showing the interaction of the edge dislocation with the emitted dislocations under the indentation surface.

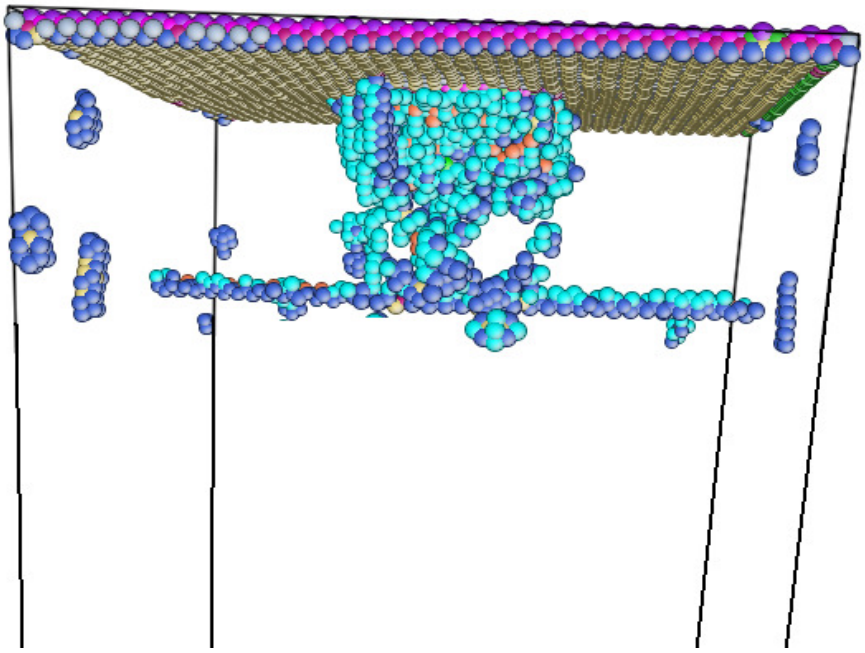

Fig. 4-4: Edge dislocation in the (1 1 -2) plane while indenting in the Z <1 1 -2> direction, yielding at a depth of 8 A. Atoms with a co-ordination number less than 8 are shown. All other atoms are removed.

Now performing nanoindentation in the same direction as the direction of motion of the edge dislocation <111> in order to show the behavior of the dislocation in such conditions, so we perform nanoindentation in the y direction <111> using the same indenter tip radius and the same indentation velocity; in this case the dislocation moves in the y <111> direction until it recombines with the surface under the indenter as shown in Fig. 4-5 and Fig. 4-6.

The motion of the dislocation toward the free surface is associated with the force of its image dislocation or image force; this force is an attraction force and is obtained from the stress of the image dislocation, it arises solely from the change in the elastic energy in the crystal:

$F_y/L= (\mu b^2)/ [(4\Pi (1-\nu) l]$ [[51]].

For iron the shear modulus, μ, is 82 Gpa and the burger's vector, b, is 0.248 nm, l is the distance from the surface 7.5 nm and L is the length of the dislocation 15 nm and poison's ratio, is 0.29. Therefore, for this simulation Fy/L= 0.0753 N/m.

The force exerted by the indenter F_i on the dislocation, considering the maximum shear stress under the indenter of around 7Gpa is on the order of

Fi/L=105 N/m. Therefore, the motion of the dislocation in the simulation is likely related to the indentation rather than resultant image forces.

It also gives an insight on the difference in the velocity of motion of the dislocation which is 273 m/s without the applied stresses of the indenter and around 600m/s when the indenter's stresses are applied.

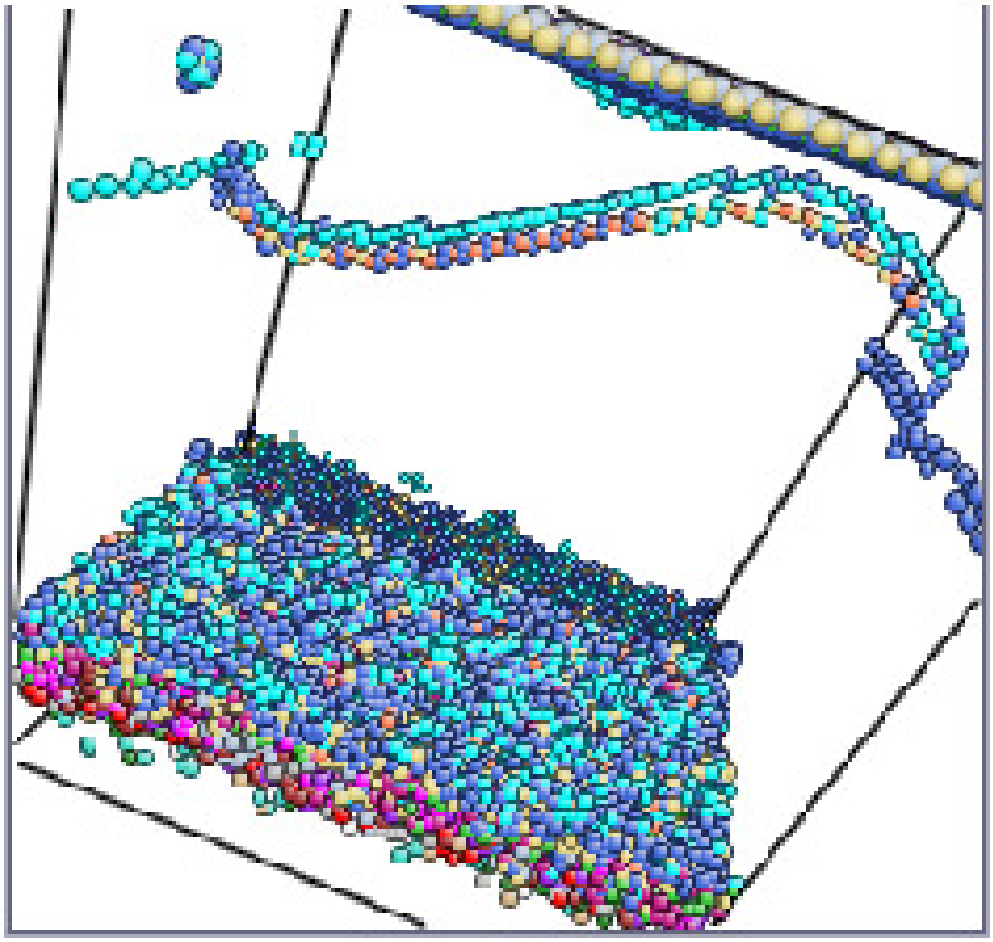

Fig. 4-5: Snapshot of atoms in simulation cell with an edge dislocation moving toward the indenter when indenting in the y <111> direction. (Depth = 5A). Atoms with a co-ordination number less than 8 are shown. All other atoms are removed.

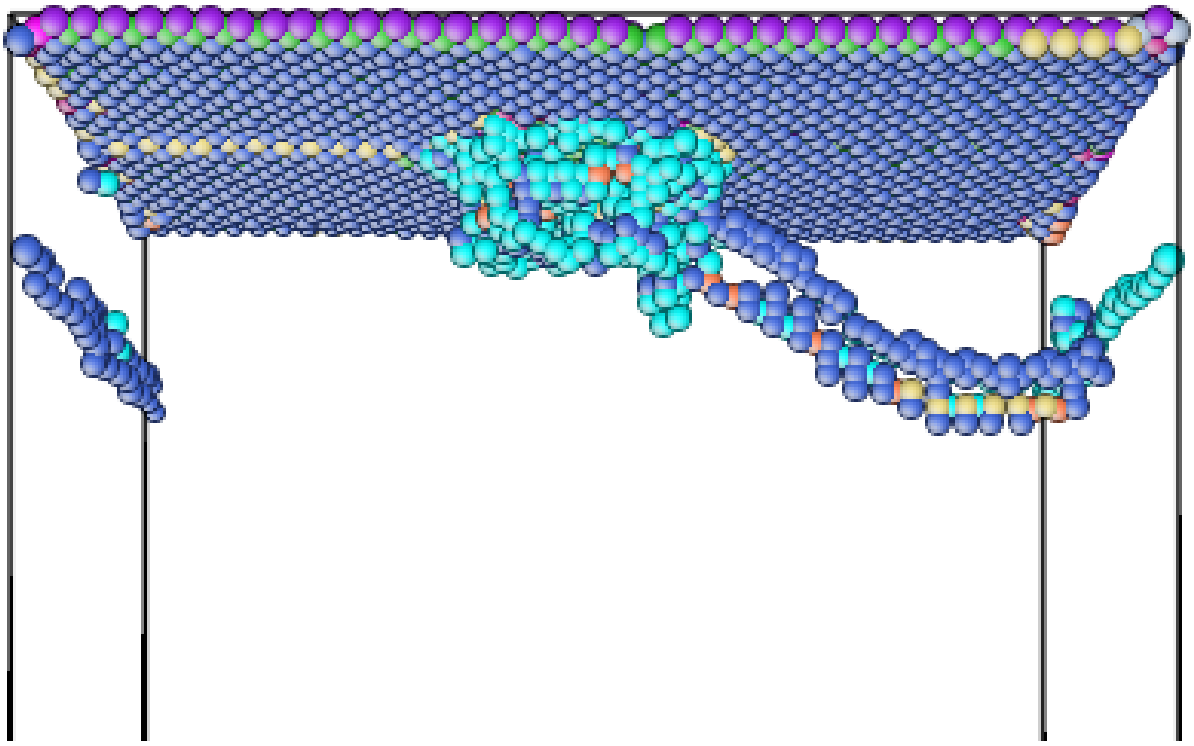

Fig.4-6: Simulatin showing dislocation moving in the <111> direction and joining the dislocations nucleating under the indenter tip (depth = 7 A). Atoms with a co-ordination number less than 8 are shown. All other atoms are removed.

Even though the dislocation moved toward the indentation surface and annihilated, we still see a decrease in the yield load due to the initial presence of the dislocation, which proves that in both cases either indenting in the <11-2> direction or the <111> direction the dislocation effect is pretty much the same, lowering the yield load during nanoindentation.

Fig. 4-7 shows the load displacement curves for all four cases: nanoindentation in the Z direction without and with dislocation, and nanoindentation in the Y direction with and without a dislocation.

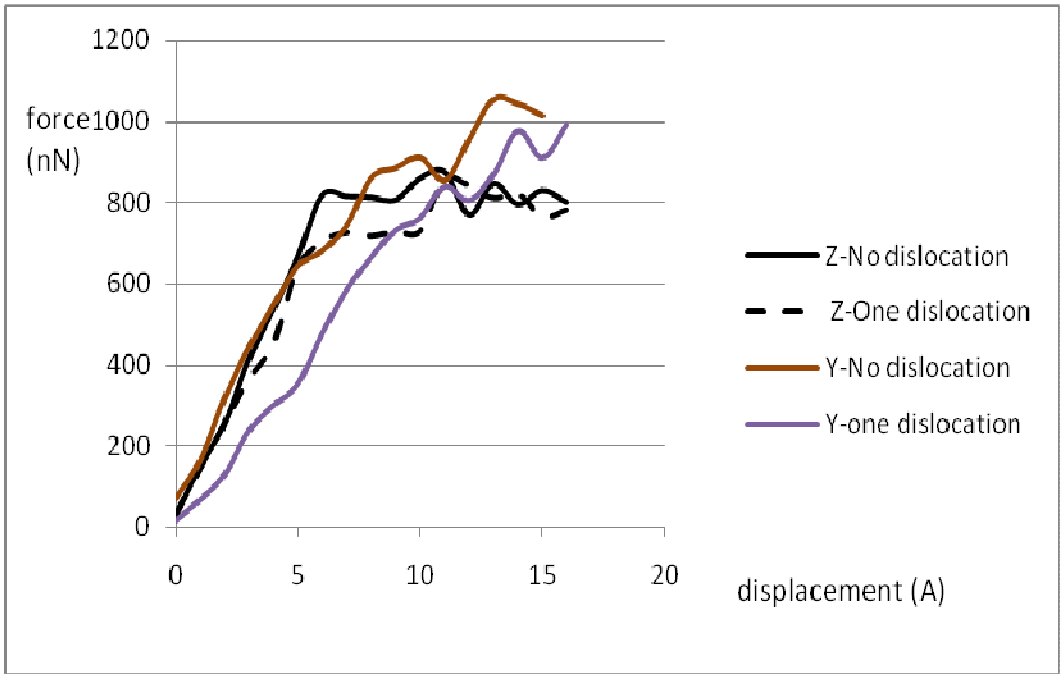

Fig. 4-7: Force displacement curves for nanoindentation in the Y and Z direction with and without a dislocation

Chapter 5 *Conclusion*

Defects in metals have been extensively studied in this thesis; their effect on mechanical properties was focus, as a result of our studies vacancies and dislocations were proved to lower the yield strength and a higher concentration of vacancies caused a higher decrease in the yield load, when applying stress to the simulation cell vacancies tend to move toward boundaries or recombine with nucleating dislocations from under the indenter tip, in other words vacancies tend to move to higher stress zones inside the simulation cell, on the other hand the edge dislocation during nanoindentation behaved as expected when it stayed fixed without motion while indenting normally to its direction of motion, and moved toward the higher stress zone ((11 -2) plane) when indenting in the same direction as its direction of motion.

Irradiation damage modeled in Zirconium HCP showed the evolution of vacancies and interstitials with time after the excitation of the PKA and quantified the number of stable defects as a function of the PKA energy and the simulation temperature, as the number of defects increased with both increasing PKA energies and increasing temperatures.

Nanoindentation was the means that we used in order to study the effects of different defects; in fact nanoindentation was a really helpful method to extract the mechanical properties of metals, with a wide feedback from literature and from experiments that clarify the right path to follow.

Molecular dynamics as a method was helpful when creating defects and even when varying conditions like temperature or strain rate; computations of nanoindentation using Molecular Dynamics were interesting due to the flexibility that MD provides when it comes to following the evolution of defects and their interactions, and it was helpful in providing insight on important phenomena during testing like the onset of plasticity.

References

[1]D. B. Shan, L. Yuan, Z. H. Xu, and B. Guo, Atomistic Simulation of Voids effect on Nanoindetation, Nanosci. Technol., 9 , 1234-1236, (2009)

[2] B.D. Wirth, M.J. Caturla, T. Diaz de la Rubia, T. Khraishi, H. Zbib, Mechanical property degradation in irradiated materials: A multiscale modeling approach, NIM B , 180, 23-31, (2001)

[3] S. Mukherjee, T. Khraishi and Y-L. Shen, Modeling the effects of particles, interstitials, vacancies and tip geometry on indentation-induced plasticity, Molecular Simulation, 32, 651-656, (2006)

[4] S.J. Plimpton, Fast parallel algorithms for short-range molecular dynamics, Journal Comput. Phys., 117, 1-19, (1995)

[5] Jinpeng Chang, Vasily V. Bulatov and Sidney Yip, Molecular dynamics study of edge dislocation motion in a bcc metal, Journal of Computer- Aided Materials Design, 6, 165-173, (1999)

[6] Qizhen Li, Effect of dislocation source length on yield strength of nanostructured metallic multilayer thin films, Materials Science and Engineering A , 493, 288-291, (2008)

[7] E.S. Altshuler , D.L. Mills, R.B. Gerber, Simulations of hydrogen diffusion on BCC metal (110) surfaces; coverage and temperature dependence, Surface Science, 452, 95–107, (2000)

[8] Farid F. Abraham, Crack dynamics in brittle fracture: An atomistic study, Nuclear Instruments and Methods in Physics Research Section B: Beam Interactions with Materials and Atoms, 180, 72-76, (2001)

[9] C. A. Schuh, J.K. Mason AND A.C. Lund, Quantitative insight into dislocation nucleation from high-temperature nanoindentation experiments, Nat. Mater. 4, 617-621, (2005)

[10] J. Chen, W. Wang, L.H. Qian, K. Lu, Critical shear stress for onset of plasticity in a nanocrystalline Cu determined by using nanoindetation, 49, 645-650, (2003)

[11] A. Gouldstone, K. J. Van Vliet, S. Suresh, Simulation of defect nucleation in a crystal, Nature 411, 656, (2001)

[12] D.M. Clatterbuck, D.C. Chrzan, J.W. Morris Jr., The ideal strength of iron in tension and shear, Acta Mater., 51, 2271-2283, (2003)

[13] Streett WB, Tildesley DJ, Saville G.,Multiple time-step methods in molecular dynamics. Mol Phys 35,639-648, (1978)

[14] D.F. Bahr, D.E. Kramer, and W.W. Gerberich, FILM FRACTURE CONTROLLED EXCURSIONS IN OXIDE - METAL SYSTEMS, Acta Mater. ,46, 3605 (1998)

[15] K. Durst, B. Backes, O. Franke, M. Goken, Acta Mater. 54 (2006) 2547

[16] Y. M Wang, A. M. Hodge, J. Biener, and A. V. Hamza, D.E. Barnes and Kai Liu, T. G. Nieh, Appl. Phys. Lett. 86 (2005) 101915

[17] D.F. Bahr, D.E. Wilson, and D.A. Crowson, J. Mater. Res. 14 (1999) 2269

[18] AM Minor, SAS Asif, ZW Shan, EA Stach, E Cyrankowski, TJ Wyrobek, OL Warren, Nature Mater., 5 (2006) 697

[19] JA Zimmerman, CL Kelchner, PA Klein, JC Hamilton, and SM Foiles, Phys. Rev. Lett. 87 (2001) 165507

[20] S.A. Syed Asif and J.B. Pethica, Phil. Mag. A 76 (1997) 1105

[21] A.B. Mann and J.B. Pethica, App. Phys. Lett. 69 (1996) 907

[22] I-Ling Chang and Yu-Chiao Chen, Nanotechnology 18 (2007) 315701

[23] M.I. Mendelev, S. Han, D.J. Srolovitz, G.J. Ackland, D.Y. Sun and M. Asta, Phil. Mag. A83 (2003) 3977

[24]J.H. Schneibel, Strengthening of iron aluminides by vacancies and or nickel, Materials Science and Engineering A, 258, 181-186, (1998)

[25] George Z. Voyiadjis *, Farid H. Abed, A coupled temperature and strain rate dependent yield function for dynamic deformations of bcc metals, International Journal of Plasticity, 22, 1398–1431, (2006)

[26] Te-Hua Fang, Sheng-Rui Jian and Der-san Chuu, Molecular Dynamics Aanalysis of Effects of Velocity and Loading on the Nanoindentation, J. Appl. Phys., 41, 1328-1331, (2002)

[27] J. Schiotz, Scr. Mater. 51 (2004) 837

[28] L. Ma , D.J. Morris, S.L. Jennerjohn, D.F. Bahr and L.Levine, J. Mater. Res. 61 (2009) 56

[29] E.H. Yoffe, Phil. Mag. A 50 (1984) 813

[30] Johnson, K. L., *Contact mechanics.* Cambridge University Press, 6. Nachdruck der 1. Auflage, (2001).

[31] R. S. Averback and T. Diaz de la Rubia, Displacement damage in irradiated metals and semiconductors, Solid State Physics, 51, 281--402, (1998)

[32]R. Smith , Atomic & ion collisions in solids and at surfaces: theory, simulation and applications, Cambridge University Press, Cambridge, UK, (1997)

[33] J. P. Crocombette, Cascade modeling, Handbook of Materials Modeling, 987-998, (2005)

[34] K. Nordlund, Atomistic Simulation of radiation effects in carbon-based materials and nitrides, Nuclear Instruments and Methods in Physics Research B , 218, 9-18, (2004)

[35] Hiroshi Shibamoto, Akihiko Kimura, Masayuki Hasegawa, Hideki Matsui, and Sadae Yamaguchi, Effects of Proton Irradiation on Reactor Pressure Vessel Steel and its Model Alloys, Journal of ASTM International, October , 2,(2005)

[36] G. R. Odette and B. D. Wirth, Radiation effects in fission and fusion reactors, Handbook of Materials Modeling, 999-1037, (2005)

[37] M.I. Mendelev and G.J. Ackland, Phil. Mag. Letters, 87, 349-359 (2007)

[38] Carlos Campañá and K. P. Boyle, Ronald E. Miller, Grain boundary motion assisted via radiation cascades in bcc Fe, PHYSICAL REVIEW B, 78, 134114-134122, (2008)

[39] A. M. Rutherford and D. M. Duffy, The effect of electron-ion interactions on radiation damage simulations, Journal of Physics and Condensed Matter, 19, 496201-496210, (2007)

[40] Na-Young Park, Yu-Chan Kim, hyun-Kwang Seok, Seung-Hee Han, Seugyon Cho and Phil-Ryung Cha, Molecular Dynamics simulation of irradiation damage in tungsten, Nuclear Instruments and Methods in Physics Research Section B: Beam Interactions with Materials and Atoms, 265, 547-552, (2007)

[41] Graig R Barret,William D Nix and Alan T. Tetelman, The principles of engineering materials (1973)

[42] Private Communication with NARASIMHAN SWAMINATHAN, Post Doctoral Research Associate at University of Wisconsin-Madison

[43] R. D. Schrimpf, D. M. Fleetwood, Radiation effects and soft errors in integrated circuits and electronic devices, 142 (2004)

[44] L. Yang, X.T. Zu, H.Y. Xiao, F. Gao, H. L. Heinisch, R. J. Kurtz, Defect production and formation of helium-vacancy clusters due to cascades in α-iron, Physics B, 391, 179-185, (2007).

[45]E.Z Orowan, Z. Phys.,89 605 (1934)

[46]G.I. Taylor, The Mechanism of Plastic Deformation of Crystals Proc. R. Soc. London 145 A , 362, (1934)

[47] H. G. M. Kreuzer and R. Pippan, Discrete dislocation of nanondentation: The effect of statistically distributed dislocations, Materials Science and Engineering A, 400-401, Pages 460-462, (2005)

[48] M.I. Mendelev, S. Han, D.J. Srolovitz, G.J. Ackland, D.Y. Sun, and M. Asta, "Development of new interatomic potentials appropriate for crystalline and liquid iron," Phil. Mag., 83, 3977-3994 (2003)

[49] G. Monnet , D. Terentyev, Structure and mobility of the ½ <111> {112} edge dislocation in BCC iron studied by molecular dynamics, Acta Materialia, 57, 1416-1426, (2009)

[50] A.A. ZBIB and D.F. BAHR, Dislocation Nucleation and source Activation during Nanoindentation Yield Points, Metallurgical and Materials Transactions A, 38A, 2249-2255, (2007)

[51] John Price Hirth and Jens Lothe, Theory of dislocations, Second Edition (1982)